Prelamin A causes progeria through cell-extrinsic mechanisms and prevents cancer invasion

Jorge de la Rosa[1], **José M. P. Freije**[2], **Rubén Cabanillas**[1], **Fernando G. Osorio**[2], **Mario F. Fraga**[3], **M. Soledad Fernández-García**[4], **Roland Rad**[5,6,7], **Víctor Fanjul**[2], **Alejandro P. Ugalde**[2], **Qi Liang**[7], **Haydn M. Prosser**[7], **Allan Bradley**[7], **Juan Cadiñanos**[1,7,*], and **Carlos López-Otín**[2]

[1]Instituto de Medicina Oncológica y Molecular de Asturias (IMOMA), 33193-Oviedo, Spain.

[2]Departamento de Bioquímica y Biología Molecular, Facultad de Medicina, Instituto Universitario de Oncología (IUOPA), Universidad de Oviedo, 33006-Oviedo, Spain.

[3]Unidad de Epigenética del Cáncer, IUOPA, Universidad de Oviedo, 33006-Oviedo, Spain.

[4]Unidad de Histopatología Molecular, IUOPA, Universidad de Oviedo, 33006-Oviedo, Spain.

[5]Department of Medicine II; Klinikum Rechts der Isar; Technische Universität München, 81675 Munich, Germany.

[6]German Cancer Consortium (DKTK), German Cancer Research Center (DKFZ), 69120 Heidelberg, Germany.

[7]The Wellcome Trust Sanger Institute, Wellcome Trust Genome Campus, Hinxton, Cambridgeshire, CB10 1SA, UK

Abstract

Defining the relationship between ageing and cancer is a crucial but challenging task. Mice deficient in Zmpste24, a metalloproteinase mutated in human progeria and involved in nuclear prelamin A maturation, recapitulate multiple features of ageing. However, their short lifespan and serious cell-intrinsic and cell-extrinsic alterations restrict the application and interpretation of carcinogenesis protocols. Here we present Zmpste24 mosaic mice that lack these limitations. Zmpste24 mosaic mice develop normally and keep similar proportions of Zmpste24-deficient (prelamin A accumulating) and Zmpste24-proficient (mature lamin A containing) cells throughout life, revealing that cell-extrinsic mechanisms are preeminent for progeria development. Moreover, prelamin A accumulation does not impair tumour initiation and growth, but it decreases the incidence of infiltrating oral carcinomas. Accordingly, silencing of *ZMPSTE24* reduces human cancer cell invasiveness. Our results support the potential of cell-based and systemic therapies for progeria and highlight ZMPSTE24 as a new anticancer target.

Introduction

Ageing and cancer are divergent consequences of the accumulation of molecular alterations with time. These changes activate cell senescence or apoptosis to prevent cancer, collaterally reducing fitness and regenerative potential [1]. The study of the ageing-cancer relationship is hampered by its complexity and duality, as ageing is caused by systemic and cellular alterations, and age is the main cancer risk factor. Disruption of the nuclear lamina, one of the cellular changes involved in natural ageing [2], underlies different syndromes known as progeroid laminopathies [3]. Hutchinson-Gilford progeria syndrome (HGPS), mandibuloacral dysplasia and restrictive dermopathy are caused by lamin A maturation defects due to mutations in the *LMNA* and the *ZMPSTE24* loci, the latter encoding the metalloproteinase required for prelamin A processing [4-7]. Altered lamin A processing has been linked to senescence and upregulation of p53-targets, telomere erosion, defective DNA repair, increased autophagy, deregulated miRNA expression, epigenetic changes and overactivation of NF-κB signalling at the cellular level [8-14]. At the systemic level, prelamin A isoforms cause alterations in the somatotroph axis, changes in glucose and lipid metabolism, and induction of chronic inflammatory responses [14,15].

The wide and large effect of alterations of lamin A and its precursors on pathways central for the control of cell viability and systemic homeostasis processes, which are very frequently altered during oncogenesis, makes a potential link of nuclear lamins with cancer very plausible. However, the studies conducted so far have not established a clear connection [16].

Zmpste24-deficient and *Lmna* knock-in mice have been successfully used as models to study progerias and test potential treatments for them [17-19]. Unfortunately, these mice have important limitations which restrict the study of the relevance of prelamin A in cancer: their shortened lifespan (4 months) is not compatible with conventional tumour induction protocols, and their concomitant systemic and cellular abnormalities make it difficult to dissect the effects of prelamin A on tumour biology [4]. To circumvent these limitations, we describe herein the generation of a novel mosaic mouse model in which Zmpste24-deficient cells –accumulating prelamin A– and Zmpste24-proficient cells – expressing mature lamin A– coexist in similar proportions within the same individual, showing no overt phenotype and normal levels of systemic parameters typically altered in progeroid mice. Moreover, this model allowed us to analyze the effects of prelamin A on tumour establishment and progression *in vivo*.

Results

Zmpste24 mosaic mice display no progeroid phenotype

We have generated a novel epigenetic-mosaic mouse model using recombination mediated cassette exchange (RMCE) (Fig.1a and Supplementary Fig. S1a), following a previously described strategy [20]. The mice in this study were *Zmpste24$^{-/-}$Hprt$^{Z24/+}$* females (hereafter "mosaic"): null for the autosomal *Zmpste24* locus, but containing an extra copy of the *Zmpste24* gene introduced at the *Hprt* locus of their X chromosome (Fig. 1a and Suppplementary Fig. S1a). Due to random X inactivation, two types of cells should be present in them: those expressing *Zmpste24* from their *Hprt* locus, and those not expressing *Zmpste24* at all. As controls, we generated *Zmpste24$^{+/-}$ Hprt$^{Z24/+}$*females (hereafter "HT-control"), which are heterozygous for the autosomal *Zmpste24* locus and thus would lack any deleterious phenotype [4], and *Zmpste24$^{-/-}$ Hprt$^{\Delta Z24/+}$* females (hereafter "KO-control"), which contain an insert in the *Hprt* locus (Δ*Z24*) similar to the one in *Zmpste24$^{-/-}$Hprt$^{Z24/+}$* mice, but missing essential *Zmpste24* coding sequences (Fig. 1a and Supplementary Fig.

S1b). To facilitate the monitoring of X inactivation, we also introduced into the *Hprt* locus a CAGGS-DsRed reporter cassette in *cis* with the *Zmpste24* and Δ*Z24* inserts (Supplementary Fig. S1a,c). Mosaic, HT-control and KO-control mice were born at the expected Mendelian ratios.

To ascertain the production of functional Zmpste24 metalloproteinase from the *Zmpste24* gene at the *Hprt* locus, we obtained protein extracts from mosaic pups and performed lamin A and prelamin A Western blot analysis. Whereas in the presence of autosomal *Zmpste24* (HT-control) just lamin A was detected, and in its absence (KO-control), only prelamin A was observed, extracts from newborn ear mosaic fibroblasts contained lamin A and prelamin A, consistent with the co-existence of Zmpste24-deficient and -proficient cells (Fig. 1b). Interestingly, mosaic mice were phenotypically indistinguishable from wild-type or HT-controls, as they did not present the progeroid phenotypes and shortened lifespan of *Zmpste24*^{−/−} or KO-control mice (Fig. 1c-f). These results indicate that mosaic Zmpste24 complementation generates lamin A-expressing cells which elicit reversion of the progeroid phenotype induced by prelamin A in *Zmpste24*-deficient mice.

Zmpste24-deficient and -proficient cells thrive equally

To evaluate the persistence of prelamin A-expressing cells in mosaic mice, we performed DsRed fluorescence analysis of different organs. Prelamin A-containing cells display replicative defects in *Zmpste24*-deficient mice [11]. If this was the case in mosaic mice, we should detect a replacement of cells not expressing Zmpste24 by those expressing this metalloprotease. Interestingly, all organs studied from 1-year-old mosaic mice, double the maximum lifespan of *Zmpste24*^{−/−} mice, contained fluorescent (DsRed positive) and non-fluorescent cells (Fig. 2a). Furthermore, immunohistochemical labelling of DsRed and prelamin A in hearts from mosaic mice confirmed that DsRed-expressing cells contained Zmpste24 able to process prelamin A, whereas this lamin A precursor was accumulated in DsRed-negative cells (Fig. 2b). To analyze whether cell substitution occurred with age, we dissected tissues from 2-month, 1-year and 2-year-old mice and measured their DsRed fluorescence. We did not detect significant changes in the intensity of red fluorescence in any organ except for the heart, where a consistent increase of DsRed signal was apparent (Fig. 2c). However, this increase was also detected in HT-control and in *Zmpste24*^{+/−}*Hprt*[ΔZ24/+] animals, which only contain Zmpste24-proficient cells, ruling out the possibility that it was related to the effects of prelamin A (Supplementary Fig. S2). Then, as red fluorescence is an indirect reporter of Zmpste24 expression, we confirmed our results by immunoblotting of Zmpste24, lamin A and prelamin A in tissues from 4-, 12- and 24-month-old mice (Fig. 2d and Supplementary Fig. S3). Consistently, no significant changes on the levels of these proteins were detected.

To finely measure the proportions of Zmpste24-deficient and -proficient cells in different tissues with age we pyrosequenced bisulfite-modified DNA. This approach allowed us to detect methylation of specific CpG dinucleotides in the *Zmpste24* promoter located at the *Hprt* locus, which shows maximum levels of methylation in the inactive X chromosome (Fig. 3a). To set the maximum methylation value, we analyzed two lines of *Zmpste24*-deficient ear fibroblasts isolated from mosaic mice by random drift during serial passages in culture (Fig. 3a). These cells only produce prelamin A, thereby representing the highest level of methylation observable. CpG 3 and CpG 4 dinucleotides showed methylation values consistently high in these *Zmpste24*-deficient cells. We focused on CpG 3 and set the 100% methylation level as the average value obtained for this dinucleotide in *Zmpste24*-deficient cells. As expected, CpG 3 methylation in all tissues from wild-type mice was negligible (Fig. 3a). We then analyzed tissues from mosaic mice and HT-control mice (Fig. 3b). If substitution of *Zmpste24*-deficient by -proficient cells occurred, the percentage of methylation in the *Zmpste24* promoter should decrease with age in the mosaic mice.

However, methylation levels did not decrease significantly with time in mosaic tissues, and remained similar to the values obtained in HT-control tissues between 2 months and 2 years, including the heart (Fig. 3b).

To further explore these *in vivo* observations we studied whether the presence of wild-type cells is able to rescue the phenotype of Zmpste24-deficient fibroblasts *in vitro*. The growth dynamics of co-cultures of adult fibroblasts (AFs) explanted from wild-type and Zmpste24 knock-out mice closely resembled that of wild-type AFs, suggesting that Zmpste24-deficient AFs proliferate better in the presence of wild-type cells (Supplementary Fig. S4a). To analyze whether, as previously reported for LMNAΔ9 mouse AFs [21], the presence of extracellular matrix (ECM) alone was able to rescue the proliferative ability of Zmpste24-deficient AFs, we cultured them on ECM previously deposited by wild-type or Zmpste24-deficient AFs. Interestingly, both types of ECM improved the replicative capacity of Zmpste24-deficient AFs, suggesting that an ECM production deficit, and not the lack of specific components of the ECM, underlies the reduced proliferative ability of Zmpste24-deficient cells *in vitro* (Supplementary Fig. S4b).

Taken together, these results indicate that prelamin A accumulation does not represent a selective disadvantage for cells of mosaic mice, where Zmpste24-deficient and -proficient cells coexist in similar proportions, and suggest that ECM-mediated mechanisms contribute to the reversal of the phenotype of Zmpste24-deficient cells.

Progeria markers are rescued in mosaics

Because p53-target genes are overexpressed in hearts from *Zmpste24*^{−/−} mice [11], we analyzed cardiac *p21, Atf3* and *Igfbp3* mRNA levels in mosaic mice. Whereas *Zmpste24*-deficient hearts showed overexpression of these three p53-target mRNAs, the levels of these transcripts were normal in mosaic hearts (Fig. 4a). To further explore this observation, we used DsRed labelling to separate Zmpste24-deficient from -proficient cells by microdissection of mosaic hearts. Interestingly, *p21* and *Igfbp3* levels were not significantly different in Zmpste24-deficient and -proficient cardiomyocytes from the same mosaic mouse (Fig. 4b). Together, these results indicate that the upregulation of p53-target transcripts in Zmpste24-deficient mice is not a direct consequence of prelamin A accumulation in each cell, but likely secondary to the progressive organismal deterioration of these animals. We next analyzed the levels of biochemical markers and hormones deregulated in the complete absence of Zmpste24 [11,15]. IGF1, glucose and major urinary protein (MUP) levels were normal in mosaic mice (Fig. 4c,d). Thus, these animals appear healthy, despite containing a high proportion of prelamin A-expressing, Zmpste24-deficient cells. All these observations further support the idea that cell-extrinsic mechanisms are preeminent in the onset and development of prelamin A-induced progeria.

Prelamin A accumulation does not affect tumour initiation

As Zmpste24 mosaic mice contain prelamin A-expressing cells in a normal environment, we used them to evaluate the potential role of A-type lamins in cancer. To compare the tumour initiation potential of prelamin A-expressing cells and normal lamin A-expressing cells, we performed two protocols: topical DMBA-TPA application for the induction of skin papillomas [22] and urethane injection for the generation of lung adenomas [23]. We did not detect differences in tumour susceptibility between HT-control and mosaic mice or in the number of tumours expressing or lacking prelamin A in the latter animals (Supplementary Fig. S5a-c). Consistent with these observations, no significant differences in Ki67 staining were detectable between prelamin A-positive and -negative tumours (Supplementary Fig. S5d). Thus, prelamin A does not affect the susceptibility of epithelial cells from the skin or lung to neoplasia.

Prelamin A accumulation prevents cancer invasion

To test whether prelamin A could play a role in cancer progression, we performed an additional carcinogenesis protocol based on the administration of 4-nitroquinoline 1-oxide (4-NQO) in drinking water to induce squamous cell carcinomas of the upper digestive tract [24]. This protocol produced a wide spectrum of neoplastic lesions, from benign papillomas to infiltrating carcinomas. In agreement with the above results, no differences were observed in premalignant lesions (Fig. 5a). However, the proportion of mosaic mice affected by infiltrating carcinomas of the oral cavity was significantly reduced, as compared to HT-controls (Fig. 5a). Moreover, the proportion of oral infiltrating carcinomas with respect to all carcinomas (carcinomas in situ plus infiltrating carcinomas) was also strikingly lower in the mosaic mice (Fig. 5b). Interestingly, whereas the numbers of carcinomas in situ expressing and not expressing prelamin A by immunohistochemistry were comparable in mosaic mice (Fig. 5c), the only two infiltrating carcinomas observed in these animals lacked prelamin A staining (Fig. 5d).

To explore the mechanistic basis of this observation in a human cancer context, we used siRNAs to silence *ZMPSTE24* in cell lines from human infiltrating oral carcinomas (SCC-40 and SCC-2), and compared their RNA expression profiles with those of mock treated cells. *ZMPSTE24* silencing produced prelamin A accumulation and induced relevant changes in gene expression. Interestingly, gene set enrichment analysis revealed that among the pathways most significantly altered in *ZMPSTE24*-silenced SCC-40 and SCC-2 cells are those involved in ECM composition and in cell-ECM interactions (Supplementary Tables S1-S3). This observation, together with the well-established relationship between ECM and cancer cell invasiveness, prompted us to test whether prelamin A accumulation also affected the invasive properties of these cancer cell lines. Consistent with our *in vivo* results, *in vitro* invasion assays with *ZMPSTE24*- silenced SCC-40 and SCC-2 cells showed that the accumulation of prelamin A caused a significant decrease of their invasive potential (Fig. 5e).

To study whether this effect was specific to oral cancer, we analyzed breast (MDA-MB-231) and lung (A549) cancer cells, observing a reduction in their invasive ability in the presence of prelamin A (Fig. 5e). Genome-wide expression profiles of these cells upon *ZMPSTE24*-silencing also pointed to pathways involved in the synthesis of precursors of ECM components as the most significant commonly altered molecular routes (Supplementary Table S1). Additionally, all four cell lines studied showed significant changes in expression of main components of ECM-receptor interaction pathways, such as *ITGA5*, *CD47* or *DAG1* (Supplementary Table S2). Thus, *ZMPSTE24* silencing in oral, breast and lung cancer cell lines causes prelamin A accumulation and rewiring of ECM-related cellular pathways, which could account for their reduced invasive potential. Interestingly, all four *ZMPSTE24*-silenced cancer cell lines analyzed showed alterations in routes involved in proteoglycan synthesis (chondroitin sulfate CS and/or heparan sulfate HS) (Supplementary Tables S1,S3), showing expression changes indicative of increased production of oversulfated forms of both ECM components.

Discussion

Human lifespan extension is rising the incidence of pathologies associated with age, of which cancer is the second most lethal, only after cardiovascular disease [25]. Age is the main risk factor for cancer incidence, but the links between ageing and cancer remain difficult to define due to the complex relationship between both processes [26]. Besides causing accelerated ageing syndromes, immature lamin A forms accumulate with advancing age in non-progeroid cells and have been linked to the activation of tumour suppressor

mechanisms [2,11]. Accordingly, one potential role for prelamin A would be the protection against cancer.

Due to their short lifespan, mouse models of progeroid laminopathies are not suitable for the analysis of the effects of lamin A precursors on cancer. To circumvent this limitation, we have created a novel mosaic mouse model containing prelamin A-accumulating and normal cells. These mice do not suffer from premature death and, therefore, are suitable to study the effects of this lamin A precursor on tumour initiation and progression.

Our thorough analysis of mosaic mice has revealed that prelamin A accumulation does not represent a selective disadvantage for cells, demonstrating that cell-extrinsic mechanisms are preeminent in progeria pathogenesis. This finding was unexpected, as abnormal prelamin A processing causes defects in essential cell pathways [9-11,27-32]. In line with our observations, Song et al. have recently shown that exposure of progeroid *Zmpste24*-deficient muscular derived stem/progenitor cells (MDSPCs) to wild-type MDSPCs rescues their myogenic differentiation defect *in vitro*[33]. Even in the light of this observation, the complete absence of progeroid features in our mosaic mice is a remarkable and encouraging finding.

Our results suggest that the positive effects of Zmspte24-proficient cells on Zmpste24-deficient cells are mediated by a combination of structural and diffusible factors. Thus, the replicative defects shown by *Zmpste24*-deficient AFs grown *in vitro* is rescued by the presence of ECM. This observation recapitulates the results previously obtained with LMNAΔ9 mouse AFs[21]. Additionally, circulating levels of systemic factors such as IGF1 are restored in mosaic mice. Although, from our observations, we cannot distinguish whether the normal levels of IGF1 are responsible for the lack of progeroid phenotype or a consequence of it in mosaic mice, the positive effect of the administration of this hormone to *Zmpste24*-deficient mice supports the existence of a causative role for IGF1 on the prevention of progeria[15].

Moreover, our findings highlight the potential relevance of both systemic and cell-based or gene correction treatments for progeroid syndromes and pathologies associated with normal ageing [18,34]. In this regard, parabiosis experiments, in which the circulatory systems of young and old mice are artificially connected, have already shown the potential of systemic factors to prevent certain characteristics of natural ageing [35,36]. One of these, the TGF-β superfamily member GDF11, has been recently identified as a circulating factor in young mice that declines with age and is able to reverse age-related cardiac hypertrophy when administered to old mice[35]. On the other hand, the generation of genetically corrected induced pluripotent (iPS) stem cells from HGPS fibroblasts, or the feasibility to perform *in vivo* genomic editing, create novel treatment options for these pathologies that need to be further explored [37-40]. Our results, showing that full reversion of the progeroid phenotype is compatible with the persistence of a high proportion of prelamin A-expressing cells, reinforce the potential held by gene correction and cell-based therapeutic approaches to tackle these dramatic progeroid syndromes.

Cancer induction experiments performed in mosaic mice indicate that prelamin A does not affect tumour initiation, but it prevents cancer invasion. This was confirmed in human oral, lung and breast cancer cell lines, suggesting that cancer invasion might display non-oncogenic addiction to the Zmpste24 metalloproteinase [41]. Molecular surveillance of the acquisition of invasive properties constitutes a plausible cancer control checkpoint. Thus, although the loss of p53 has no effect on the number of mutant-*Kras*-induced lung tumours or mutant-*Braf*-induced colorectal adenomas, its presence prevents the progression of benign adenomas into adenocarcinomas [42-44]. The accumulation of immature lamin A isoforms

might constitute one of those mechanisms which could become stronger with time to compensate for the increased cancer risk inherent to ageing [2].

The observed expression changes in pathways involved in ECM composition upon Zmpste24-silencing in human cancer cell lines indicate that prelamin A might exert this protective effect through a cell-extrinsic mechanism. Actually, the ECM and its interactors are main characters of cancer invasion [45]. Although increased levels of proteoglycans have been linked to enhanced invasion, recent work has shown that both CS and HS can exert different roles depending on their specific modifications (such as oversulfation) and microenvironment [46,47]. Moreover, synthetic HS mimetics have been proposed as anticancer agents able to inhibit tumour progression and metastasis, opening the possibility that specific natural HS isoforms might play similar anticancer roles [48]. The potential cell-extrinsic effect of prelamin A accumulation on prevention of cancer cell invasion is supported by the fact that the proportion of carcinomas displaying invasive properties in mosaic mice (6%) is far below half of that observed in HT-controls (39%). On the other hand, the only two oral infiltrating carcinomas observed in mosaic mice lacked prelamin A expression, and this would be consistent with a cell-autonomous effect of prelamin A on invasion prevention. Further work involving prelamin A expression analysis on a much larger number of infiltrating carcinomas will be required to clarify this issue.

In summary, we have developed a novel mosaic mouse model constituted by prelamin A-accumulating cells and mature lamin A-expressing cells in similar proportions, which shows no overt phenotype. Besides representing a useful tool for the study of the relevance of prelamin A in cancer initiation and progression, the molecular and cellular characterization of these mice highlights the importance of cell-extrinsic mechanisms for the establishment of laminopathy-based progerias. Moreover, it suggests that cell/gene therapies and supplementation of systemic factors hold great potential to tackle these degenerative diseases. These approaches could be combined with the pharmacological strategies already proven to work in animal models which are currently being evaluated in clinical trials [19]. In addition, the role of prelamin A against cancer invasion suggests that ZMPSTE24 metalloprotease could be an attractive new target for cancer therapy.

Methods

Generation of the *Hprt^{Z24}* allele

The RP23-227I2 BAC clone was modified by the introduction of a pgk/EM7-Neo/KanR-CAGGS-DsRed cassette, permitting positive selection in bacteria (with kanamycin) and eucariotic cells (with G418) and controlling the expression of the fluorescent protein DsRed. For the generation of the pgk/EM7-Neo/Kan^R-CAGGS-DsRed cassette, elements from three different plasmids were used: pCEI1, MG1 and pDsRed-Monomer-N1. pCEI1 was described in the original paper introducing the RMCE technique [20]. This plasmid contains the Neo/KanR gene controlled by the pgk/EM7 promoter and flanked by mini-arms of homology for the *sacBII* gene, which permit insertion of the resistance cassette in the BAC by homologous recombination in bacteria. The MG1 plasmid was created by H.P., and contains the CAGGS promoter from the pCAGGS vector [49], but with a more versatile cloning site. The pDsRed-Monomer-N1 plasmid (Clontech) contains the cDNA for the Monomer-N1 version of the red fluorescent protein DsRed. First, the *Not*I site from pDsRed-Monomer-N1 was destroyed. For that purpose, this plasmid was linearized by *Not*I digestion, the protruding ends were blunted with Klenow, and the plasmid was religated and transformed in competent *Escherichia coli* cells to generate pDsRed-Monomer-N1-*Not*I-Dest. After that, the MG1 plasmid was digested with *Afl*II, a 1,759 bp fragment containing the CAGGS promoter was isolated and blunted with Klenow, and that fragment was cloned into pDsRed-Monomer-N1-*Not*I-Dest which had been previously linearized with *Hin*dIII

and *Eco*RI, blunted with Klenow and dephosphorylated, to generate the pCAGGS-DsRed-Monomer-N1 plasmid. Finally, pCAGGS-DsRed-Monomer-N1 was digested with *Hin*dIII and *Afl*II to isolate a 2,750 bp fragment containing the CAGGS-DsRed-Monomer-N1 cassette, which was blunted with Klenow and cloned into pCEI1, previously linearized with *Bam*H1, blunted with Klenow and dephosphorylated. This produced the pCEI1-CAGGS-DsRed-Monomer-N1 plasmid. This plasmid can be used to introduce kanamycin/G418 resistance ability and DsRed expression into any BAC containing the *sacBII* gene. This vector was linearized with *Not*I and electroporated into electrocompetent EL350 cells which had been previously transformed with the RP23-227I2 BAC according to previously described protocols [50]. To isolate recombinant clones containing the BAC modified with the pgk/EM7-Neo/Kan[R]-CAGGS-DsRed cassette, chloramphenicol and kanamycin selection was applied (the backbone from the BAC provides chloramphenicol resistance and the pgk/EM7-Neo/Kan[R]-CAGGS-DsRed cassette provides kanamycin resistance). The identity of the BAC was checked by digestion with restriction enzymes, BAC DNA was isolated from a positive EL350 clone, and it was retransformed into DH10B bacteria for large scale isolation of the modified BAC, as previously described [20]. The *Hprt*[Z24] allele was generated following a strategy very similar to that previously described [20].

Analysis of BAC insert integrity by array CGH

Four recombinant ES cell clones (A1, A3, A10 and A12) were selected for detailed analysis of BAC insert integrity, as partial insert deletions have been described in ES cell clones generated by RMCE [20]. Insert integrity was analyzed using a custom CGH 4-plex Roche Nimblegen Array. Each of the four subfields of the array contained two different regions: a high resolution region, made of 45,000 probes evenly distributed between genomic coordinates 120627332 and 120942331 of mouse chromosome 4 excluding repetitive DNA regions (1 probe every 4 bp), and a low resolution region, consisting of 25,000 probes homogenously scattered along the whole mouse genome (1 probe every 100 kb). The high resolution region spans the whole BAC insert, plus two additional 64,171 bp-long sequences, corresponding to the mouse chromosome 4 regions flanking the sequence contained in the BAC insert at its 5′ and 3′ ends. The array-CGH results were analyzed with SignalMap, which permitted the detection of a 38,200 bp deletion in clone A2, corresponding approximately to coordinates 120742750-120780950 of mouse chromosome 4, and thus containing the first seven exons of *Zmpste24*. No alterations were observed in inserts from clones A1, A3 and A12 (Supplementary Fig. S1b).

Mouse strains

Animal experiments were conducted in accordance with the guidelines of the University of Oviedo's Committee on Animal Experimentation. Mutant mice deficient in the Zmpste24 metalloproteinase have been described previously [4]. *Hprt*[Z24] and *Hprt*[ΔZ24] mice were obtained from A3 and A2 ES cell clones, respectively (Supplementary Fig. S1b). *Zmpste24*^{−/−}*Hprt*[Z24/+] mice were obtained by crossing *Zmpste24*^{+/−} males with *Hprt*[Z24/+] females to produce *Zmpste24*^{+/−}*Hprt*[Z24] males and *Zmpste24*^{+/−}*Hprt*[Z24/+] females. These mice were backcrossed with *Zmpste24*^{+/−} mice to produce *Zmpste24*^{−/−}*Hprt*[Z24] males. Those males were subsequently backcrossed with *Zmpste24*^{+/−} mice to produce mosaics and HT-controls. *Zmpste24*^{−/−}*Hprt*[ΔZ24/+] mice were obtained by crossing *Zmpste24*^{+/−} males with *Hprt*[ΔZ24/+] females to get *Zmpste24*^{+/−}*Hprt*[ΔZ24] males and *Zmpste24*^{+/−}*Hprt*[ΔZ24/+] females, which were backcrossed with *Zmpste24*^{+/−} mice to obtain KO-controls. Mosaic mice were genotyped by a combination of conventional and quantitative PCR (Supplementary Fig. S6).

In Vivo Imaging System (IVIS)

For whole organ DsRed imaging, fresh organs were placed on black cards and analyzed for fluorescence using the IVIS system (Xenogen). DsRed was excited at 570 nm and detected at 600 nm. Data were collected and analyzed using Living Image software v3.1 (Xenogen).

Bisulfite pyrosequencing assays

Sodium bisulfite modification of 0.5 µg genomic DNA isolated from various tissues was carried out with the EZ DNA Methylation Kit following the manufacturer's protocol. Bisulfite-treated DNA was eluted in 15 µL, and 2 µL were used as template for each PCR. The set of primers for PCR amplification and sequencing were designed using a specific software pack (PyroMark assay design version 2.0.01.15). Primers were designed to hybridize with CpG-free sites to ensure methylation-independent amplification (see Supplementary Table S4). PCR was performed with biotinylated primers, to facilitate the conversion of the PCR product to single-stranded DNA templates. Vacuum Prep Tool (Biotage, Sweden) was used to prepare single-stranded PCR products according to manufacturer's instructions. Pyrosequencing reactions and methylation quantification were performed in a PyroMark Q24 System version 2.0.6 (Qiagen). Graphs of methylation values show bars identifying CpG sites with values ranging from 0% to 100%.

Blood and plasma parameters

Mice were fasted for 5 h to avoid alterations in blood parameters due to food intake previous to measurements. Blood glucose was measured with an Accu-Chek glucometer (Roche Diagnostics) using blood from the tail vein. For other parameters, blood was extracted directly from the mandibular sinus after anesthetizing mice with isoflurane. To obtain plasma, blood was centrifuged immediately after collection at $3000 \times g$ and 4 °C and the supernatant was collected and stored at -80 °C until analysis. Plasma IGF1 concentration was determined using the R&D Systems Quantikine ELISA kit, according to the manufacturer's instructions.

Carcinogenesis protocols and analysis of tumours

Mice were all female littermates aged 6-8 weeks at the start of tumour induction protocols. For the generation of skin tumours, mice were shaved and treated with a single dose of DMBA (Sigma; 25 µg in 200 µL acetone). Subsequently, mice were treated twice weekly with TPA (Sigma; 200 µL of 10^{-4} M solution in acetone) for 12 consecutive weeks. Mice were sacrificed 17 weeks after the start of treatment and tumours were either snap-frozen in liquid nitrogen or fixed and processed for histological studies. For the generation of lung tumours, mice were i.p. injected with 1 g/kg of urethane (Sigma) once a week for 8 consecutive weeks. Mice were sacrificed at 28 weeks following the initial urethane injection. Then, lungs were fixed in 4% paraformaldehyde, paraffin embedded, sectioned, and stained with H&E for morphologic examination. For the generation of upper digestive tract tumours, a stock solution of the carcinogen 4-NQO (Sigma) was prepared weekly in propylene glycol at 5 mg/mL, and stored at 4 °C. Mice were provided drinking water containing 4-NQO (100 µg/mL) ad libitum during the treatment. After a 20-week carcinogen treatment, mice were kept alive for 2 more weeks and sacrificed. Blocks containing the tongues together with the lower mandibles of mice were dissected immediately, fixed in 4% paraformaldehyde, decalcified if necessary, paraffin embedded, sectioned, and stained with H&E for pathological examination.

Gene silencing and invasion assays

For gene silencing experiments, cells were transfected with 50 nM final concentration of *ZMPSTE24* or negative control Stealth RNAi siRNAs (Life Technologies; catalogue

numbers: HSS115696 and HSS115697 for human *ZMPSTE24* and 12935-300 for negative control scramble siRNA) using Lipofectamine RNAi Max (Life Technologies) in Opti-MEM I Reduced Serum Medium without serum (Gibco) following manufacturer's instructions. In vitro invasion potential was evaluated using 24-well Matrigel-coated invasion chambers with an 8 µm pore size (BD Biosciences). For SCC-40 and A549 cell lines, 5×10^4 and 3×10^4 cells respectively were allowed to invade for 48 h using 10% fetal bovine serum as chemoattractant. In the case of SCC-2 and MDA-MB-231 cells, the invasion ability of 2.5×10^4 cells was evaluated for 24 h, using 5% fetal bovine serum as chemoattractant. Cells that reached the lower surface were stained with crystal violet and counted under the microscope.

Gene expression arrays

Global RNA expression profiling was done using Illumina HumanHT-12 version 4 beadchip. Data were quantile normalised and analysed using the bioconductor (http://www.bioconductor.org/), lumi (http://www.bioconductor.org/packages/2.0/bioc/html/lumi.html) and limma packages, then p-value was adjusted for multiple testing.

Gene Set Enrichment Analysis

GSEA was performed as described [51]. For data analysis, we used GSEA release 3.4 and MSigDB release 3.0 (http://www.broadinstitute.org/gsea/index.jsp). Weighted enrichment scores were calculated with gene expression lists ranked by signal to-noise ratio. The number of permutations was set to 1000. Analyses were focused on curated gene sets from the canonical pathway (CP) subcollection.

Supplementary Material

Refer to Web version on PubMed Central for supplementary material.

Acknowledgments

References

1. López-Otín C, Serrano M, Partridge L, Blasco MA, Kroemer G. The hallmarks of aging. Cell. 2013; 153:1194–1217. [PubMed: 23746838]

2. Scaffidi P, Misteli T. Lamin A-dependent nuclear defects in human aging. Science. 2006; 312:1059–1063. [PubMed: 16645051]

3. Burtner CR, Kennedy BK. Progeria syndromes and ageing: what is the connection? Nat. Rev. Mol. Cell. Biol. 2010; 11:567–578. [PubMed: 20651707]

4. Pendás AM, et al. Defective prelamin A processing and muscular and adipocyte alterations in Zmpste24 metalloproteinase-deficient mice. Nat. Genet. 2002; 31:94–99. [PubMed: 11923874]

5. De Sandre-Giovannoli A, et al. Lamin a truncation in Hutchinson-Gilford progeria. Science. 2003; 300:2055. [PubMed: 12702809]

6. Eriksson M, et al. Recurrent de novo point mutations in lamin A cause Hutchinson-Gilford progeria syndrome. Nature. 2003; 423:293–298. [PubMed: 12714972]

7. Navarro CL, et al. Loss of ZMPSTE24 (FACE-1) causes autosomal recessive restrictive dermopathy and accumulation of Lamin A precursors. Hum. Mol. Genet. 2005; 14:1503–1513. [PubMed: 15843403]

8. Mariño G, et al. Premature aging in mice activates a systemic metabolic response involving autophagy induction. Hum. Mol. Genet. 2008; 17:2196–2211. [PubMed: 18443001]

9. Liu B, et al. Genomic instability in laminopathy-based premature aging. Nat. Med. 2005; 11:780–785. [PubMed: 15980864]

10. Cao K, et al. Progerin and telomere dysfunction collaborate to trigger cellular senescence in normal human fibroblasts. J. Clin. Invest. 2011; 121:2833–2844. [PubMed: 21670498]

11. Varela I, et al. Accelerated ageing in mice deficient in Zmpste24 protease is linked to p53 signalling activation. Nature. 2005; 437:564–568. [PubMed: 16079796]

12. Osorio FG, et al. Nuclear envelope alterations generate an aging-like epigenetic pattern in mice deficient in Zmpste24 metalloprotease. Aging Cell. 2010; 9:947–957. [PubMed: 20961378]

13. Ugalde AP, et al. Aging and chronic DNA damage response activate a regulatory pathway involving miR-29 and p53. Embo J. 2011; 30:2219–2232. [PubMed: 21522133]

14. Osorio FG, et al. Nuclear lamina defects cause ATM-dependent NF-kB activation and link accelerated aging to a systemic inflammatory response. Genes Dev. 2012; 26:2311–2324. [PubMed: 23019125]

15. Mariño G, et al. Insulin-like growth factor 1 treatment extends longevity in a mouse model of human premature aging by restoring somatotroph axis function. Proc. Natl. Acad. Sci. U.S.A. 2010; 107:16268–16273. [PubMed: 20805469]

16. Chow KH, Factor RE, Ullman KS. The nuclear envelope environment and its cancer connections. Nat. Rev. Cancer. 2012; 12:196–209. [PubMed: 22337151]

17. Fong LG, et al. A protein farnesyltransferase inhibitor ameliorates disease in a mouse model of progeria. Science. 2006; 311:1621–1623. [PubMed: 16484451]

18. Osorio FG, et al. Splicing-directed therapy in a new mouse model of human accelerated aging. Sci. Transl. Med. 2011; 3:106ra107.

19. Varela I, et al. Combined treatment with statins and aminobisphosphonates extends longevity in a mouse model of human premature aging. Nat. Med. 2008; 14:767–772. [PubMed: 18587406]

20. Prosser HM, Rzadzinska AK, Steel KP, Bradley A. Mosaic complementation demonstrates a regulatory role for myosin VIIa in actin dynamics of stereocilia. Mol. Cell. Biol. 2008; 28:1702–1712. [PubMed: 18160714]

21. Hernández L, et al. Functional coupling between the extracellular matrix and nuclear lamina by Wnt signaling in progeria. Dev. Cell. 2010; 19:413–425. [PubMed: 20833363]

22. Abel EL, Angel JM, Kiguchi K, DiGiovanni J. Multi-stage chemical carcinogenesis in mouse skin: fundamentals and applications. Nat. Protoc. 2009; 4:1350–1362. [PubMed: 19713956]

23. Miller YE, et al. Induction of a high incidence of lung tumors in C57BL/6 mice with multiple ethyl carbamate injections. Cancer Lett. 2003; 198:139–144. [PubMed: 12957351]

24. Tang XH, Knudsen B, Bemis D, Tickoo S, Gudas LJ. Oral cavity and esophageal carcinogenesis modeled in carcinogen-treated mice. Clin. Cancer Res. 2004; 10:301–313. [PubMed: 14734483]

25. Balducci L, Ershler WB. Cancer and ageing: a nexus at several levels. Nat. Rev. Cancer. 2005; 5:655–662. [PubMed: 16056261]

26. Kirkwood TB. Understanding the odd science of aging. Cell. 2005; 120:437–447. [PubMed: 15734677]

27. Marji J, et al. Defective lamin A-Rb signaling in Hutchinson-Gilford Progeria Syndrome and reversal by farnesyltransferase inhibition. PLoS One. 2010; 5:e11132. doi:10.1371/journal.pone. 0011132. [PubMed: 20559568]

28. Rodríguez J, et al. ERK1/2 MAP kinases promote cell cycle entry by rapid, kinase-independent disruption of retinoblastoma-lamin A complexes. J. Cell. Biol. 2010; 191:967–979. [PubMed: 21115804]

29. Ragnauth CD, et al. Prelamin A acts to accelerate smooth muscle cell senescence and is a novel biomarker of human vascular aging. Circulation. 2010; 121:2200–2210. [PubMed: 20458013]

30. Cadiñanos J, Varela I, López-Otín C, Freije JM. From immature lamin to premature aging: molecular pathways and therapeutic opportunities. Cell Cycle. 2005; 4:1732–1735. [PubMed: 16258283]

31. Benson EK, Lee SW, Aaronson SA. Role of progerin-induced telomere dysfunction in HGPS premature cellular senescence. J. Cell. Sci. 2010; 123:2605–2612. [PubMed: 20605919]

32. Osorio FG, et al. Cell autonomous and systemic factors in progeria development. Biochem. Soc. Trans. 2012; 39:1710–1714. [PubMed: 22103512]

33. Song M, et al. Muscle-derived stem/progenitor cell dysfunction in Zmpste24-deficient progeroid mice limits muscle regeneration. Stem Cell Res Ther. 2013; 4:33. doi:10.1186/scrt183. [PubMed: 23531345]

34. Lavasani M, et al. Muscle-derived stem/progenitor cell dysfunction limits healthspan and lifespan in a murine progeria model. Nat. Commun. 2012; 3:608. doi:10.1038/ncomms1611. [PubMed: 22215083]

35. Loffredo FS, et al. Growth differentiation factor 11 is a circulating factor that reverses age-related cardiac hypertrophy. Cell. 2013; 153:828–839. [PubMed: 23663781]

36. Conboy IM, et al. Rejuvenation of aged progenitor cells by exposure to a young systemic environment. Nature. 2005; 433:760–764. [PubMed: 15716955]

37. Zhang J, et al. A human iPSC model of Hutchinson Gilford Progeria reveals vascular smooth muscle and mesenchymal stem cell defects. Cell Stem Cell. 2011; 8:31–45. [PubMed: 21185252]

38. Liu GH, et al. Targeted gene correction of laminopathy-associated LMNA mutations in patient-specific iPSCs. Cell Stem Cell. 2011; 8:688–694. [PubMed: 21596650]

39. Li H, et al. In vivo genome editing restores haemostasis in a mouse model of haemophilia. Nature. 2011; 475:217–221. [PubMed: 21706032]

40. Yusa K, et al. Targeted gene correction of alpha1-antitrypsin deficiency in induced pluripotent stem cells. Nature. 2011; 478:391–394. [PubMed: 21993621]

41. Freije JMP, Fraile JM, López-Otín C. Protease addiction and synthetic lethality in cancer. Frontiers in Oncology. 2011; 1:25. doi:10.3389/fonc.2011.00025. [PubMed: 22655236]

42. Junttila MR, et al. Selective activation of p53-mediated tumour suppression in high-grade tumours. Nature. 2010; 468:567–571. [PubMed: 21107427]

43. Feldser DM, et al. Stage-specific sensitivity to p53 restoration during lung cancer progression. Nature. 2010; 468:572–575. [PubMed: 21107428]

44. Rad R, et al. A genetic progression model of BRAFV600E-induced intestinal tumorigenesis reveals targets for therapeutic intervention. Cancer Cell. 2013 in press http://dx.doi.org/10.1016/j.ccr.2013.05.014.

45. López-Otín C, Hunter T. The regulatory crosstalk between kinases and proteases in cancer. Nat. Rev. Cancer. 2010; 10:278–292. [PubMed: 20300104]

46. Yang YL, et al. Influence of chondroitin sulfate and hyaluronic acid on structure, mechanical properties, and glioma invasion of collagen I gels. Biomaterials. 2011; 32:7932–7940. [PubMed: 21820735]

47. Williamson KA, et al. Age-related impairment of endothelial progenitor cell migration correlates with structural alterations of heparan sulfate proteoglycans. Aging Cell. 2013; 12:139–147. [PubMed: 23190312]

48. Basappa, et al. Anti-tumor activity of a novel HS-mimetic-vascular endothelial growth factor binding small molecule. PLoS One. 2012; 7:e39444. doi: 10.1371/journal.pone.0039444. [PubMed: 22916091]

49. Niwa H, Yamamura K, Miyazaki J. Efficient selection for high-expression transfectants with a novel eukaryotic vector. Gene. 1991; 108:193–199. [PubMed: 1660837]

50. Liu P, Jenkins NA, Copeland NG. A highly efficient recombineering-based method for generating conditional knockout mutations. Genome Res. 2003; 13:476–484. [PubMed: 12618378]

51. Subramanian A, et al. Gene set enrichment analysis: a knowledge-based approach for interpreting genome-wide expression profiles. Proc Natl Acad Sci U S A. 2005; 102:15545–15550. [PubMed: 16199517]
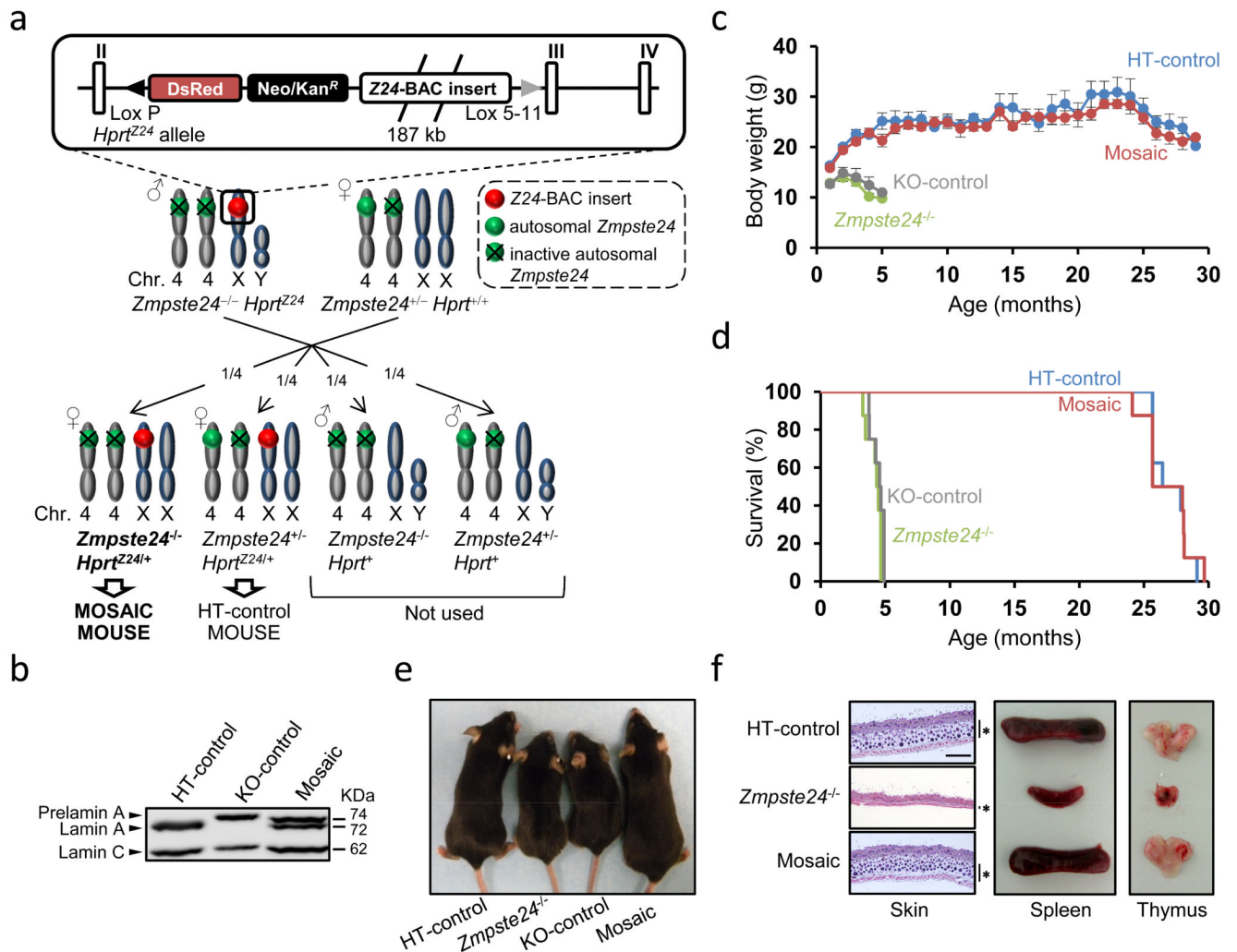
Figure 1. Absence of progeroid phenotype in Zmpste24 mosaic mice
(**a**) Breeding scheme. *Zmpste24*^{−/−}*Hprt*[Z24] males were bred with *Zmpste24*^{+/−}*Hprt*^{+/+}
females to yield female offspring that were either *Zmpste24*^{−/−}*Hprt*[Z24/+] (mosaic) or
Zmpste24^{+/−}*Hprt*[Z24/+] (HT-control). (**b**) Western blot analysis of lamins A and C from
control and mosaic neonatal fibroblasts. Original immunoblots images are shown in
Supplementary Figure S7. (**c**) Body weight vs. age of HT-control, KO-control, *Zmpste24*^{−/−}
and mosaic mice (n=5 per genotype). Error bars represent s.e.m. (**d**) Kaplan-Meier survival
plot of mice with genotypes as in (c) (n=8 per genotype). (**e**) Photographs of 4-month-old
HT-control, *Zmpste24*^{−/−}, KO-control, and mosaic mice. (**f**) Lack of progeroid features in
skin, thymus and spleen from mosaic mice. Asterisk-labelled bars indicate the depth of the
subcutaneous fat layer. Scale bar represents 500 μm.
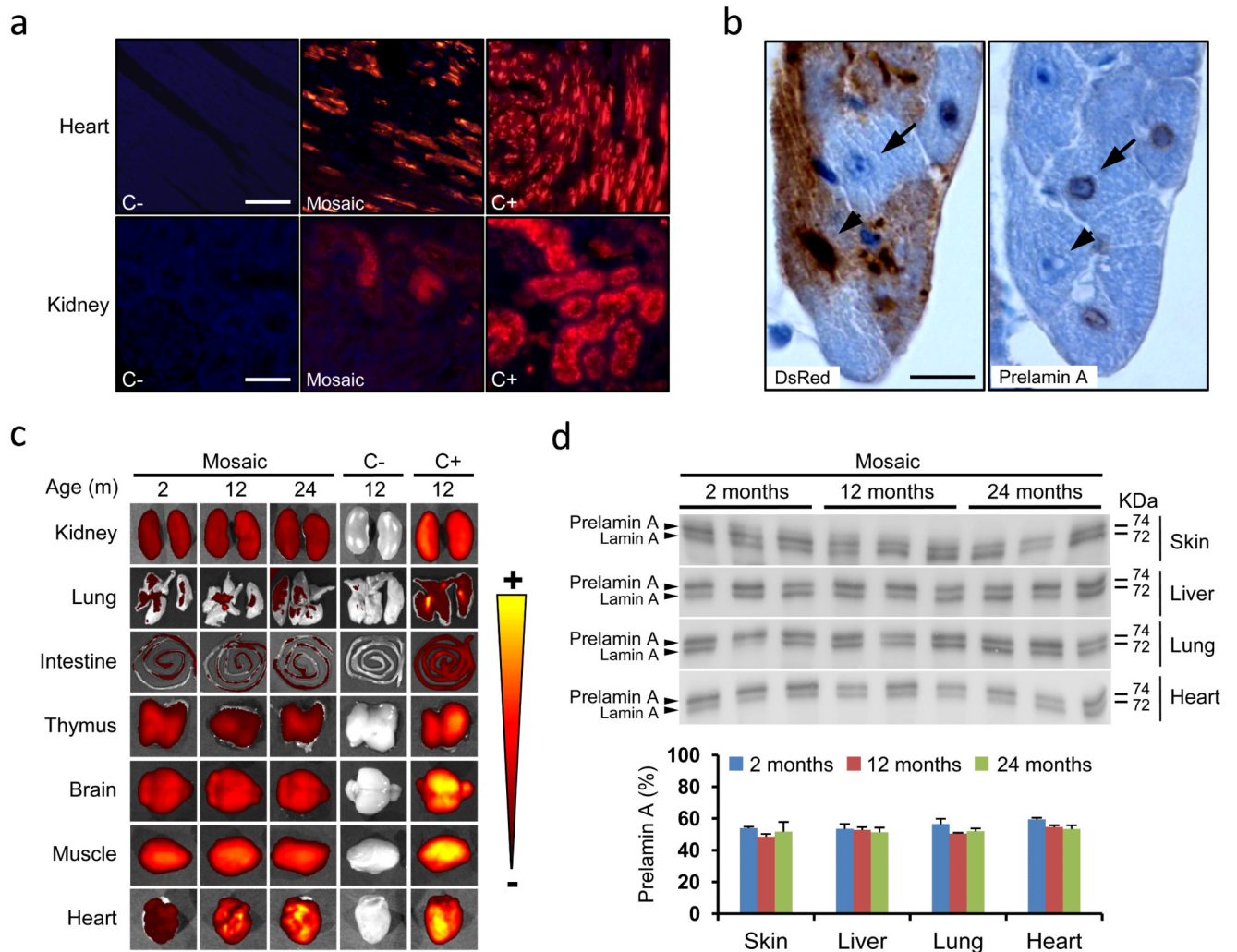
Figure 2. Zmpste24-deficient cells are detected throughout lifespan of mosaic mice
(**a**) Fluorescence microscopy of DsRed-expressing cells in tissues from
Zmpste24$^{+/+}$*Hprt*$^{+/+}$(C-), mosaic and *Zmpste24*$^{+/−}$*Hprt*$^{Z24/Z24}$ (C+) mice. Scale bars
represent 100 µm (heart) and 50 µm (kidney) (**b**) Immunohistochemical analysis of DsRed
(left) and prelamin A (right) in mosaic hearts. Arrows correspond to a Zmpste24-deficient
cell (DsRed-, prelamin A+), whereas arrowheads point to a *Zmspte24*-proficient cell (DsRed
+, prelamin A-). Scale bar represents 10 µm. (**c**) DsRed fluorescent signal detection by an In
Vivo Imaging System (IVIS) in whole organs from mosaic mice at different ages, compared
to the same organs from 1-year-old *Zmpste24*$^{+/+}$*Hprt*$^{+/+}$ (C-) and *Zmpste24*$^{+/−}$*Hprt*$^{Z24/Z24}$
(C+) mice. For comparison with DsRed signal in hearts from HT-control and
Zmpste24$^{+/−}$*Hprt*$^{ΔZ24/+}$ mice see Supplementary Figure S2. (**d**) Western blot analysis of
prelamin A and lamin A from skin, liver, lung and heart of 2-, 12- and 24- month-old mosaic
mice. A densitometry analysis of the immunoblots is also shown. Error bars represent s.e.m.
n=3.
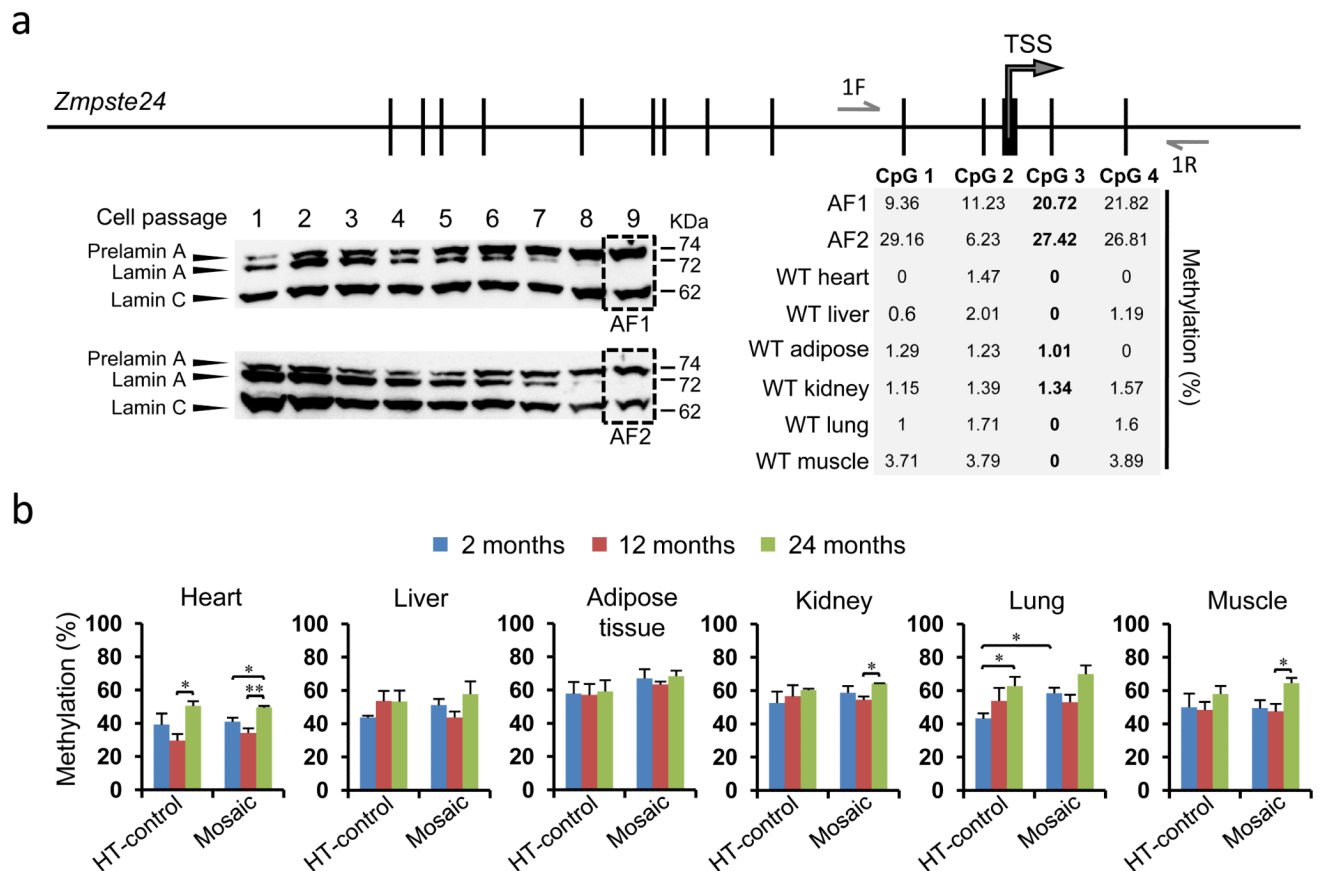
Figure 3. Mosaic mice keep similar proportions of Zmpste24-deficient and - proficient cells at all ages

(**a**) Bisulfite pyrosequencing strategy to quantify the relative proportion of Zmpste24-deficient and -proficient cells. Four CpG sites around the *Zmpste24* promoter were analyzed in DNA from Zmpste24-deficient adult fibroblasts isolated from mosaic mice (AF1, AF2) and in DNA from six wild type tissues (heart, liver, adipose tissue, kidney, lung and muscle). Western-blots show the progressive loss of mature lamin A and accumulation of prelamin A with serial passages of AF1 and AF2 cells, until only prelamin A is detected (dashed rectangles). The percent methylation of CpG sites is depicted for each of the cell populations. CpG 3 was subsequently used due to its low levels of methylation in wild-type tissues and consistent high values in the isolated fibroblasts. 1F and 1R indicate the positions of the oligonucleotides used (for sequences see Supplementary Table S4). TSS: *Zmpste24* transcription start site. (**b**) Quantitative *Zmpste24* methylation analysis by pyrosequencing in different organs from 2-, 12- and 24-month-old mosaic and HT-control mice (n 3). Error bars represent s.e.m. (*), $p < 0.05$; (**), $p < 0.01$; two tailed Student's t test.
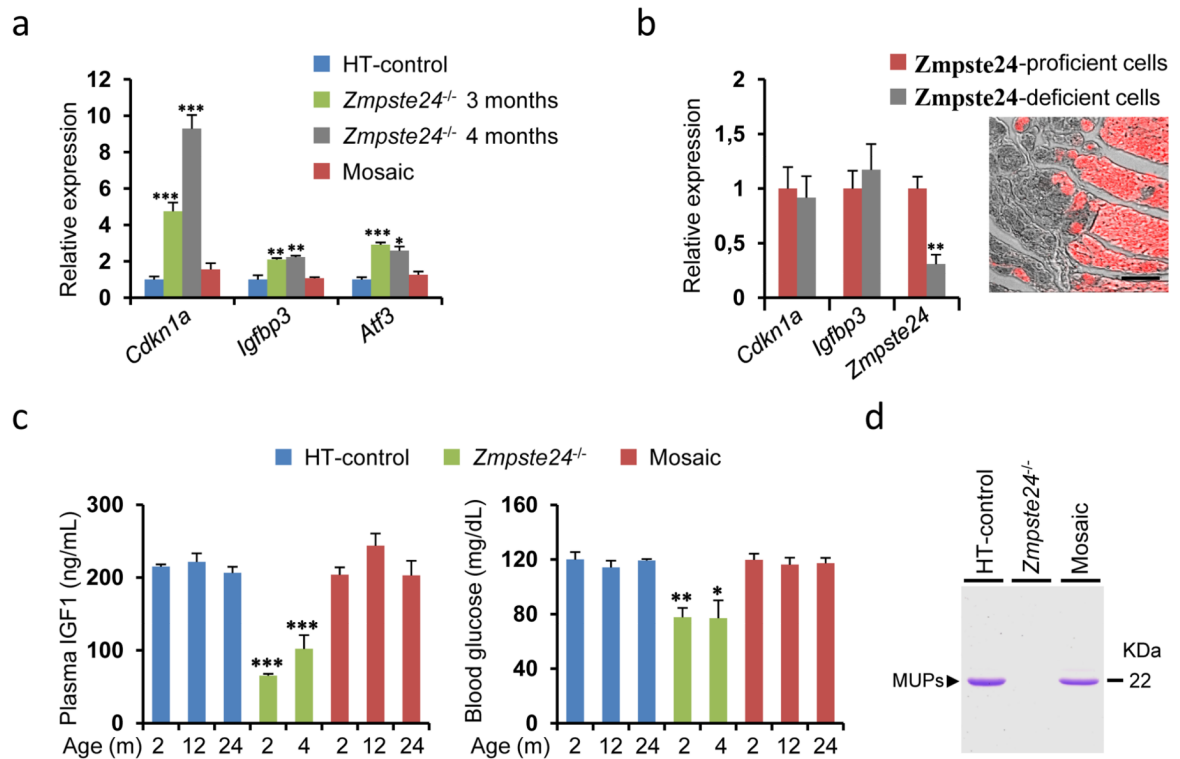
Figure 4. Rescue of molecular and systemic progeria markers in mosaic mice
(**a**) Transcriptional qPCR analysis of p53-target genes (*Cdkn1a*, *Igfbp3* and *Atf3*) in hearts from 6-month-old HT-control mice, 3-month-and 4-month-old *Zmpste24*^{−/−} and 6-month-old mosaic mice. Data are shown as fold-change values as compared to HT-controls (n 3). (**b**) Expression of *Cdkn1a*, *Igfbp3* and *Zmpste24* in microdissected DsRed fluorescent and negative cells from 6-month-old mosaic hearts (n=3). A fluorescence photomicrograph of DsRed positive (red) and negative (grey) heart areas, representative of those used for microdissection, is shown on the right. Scale bar corresponds to 100 μm. (**c**) Plasma levels of IGF1 and blood glucose concentration in HT-control, *Zmpste24*^{−/−} and mosaic mice of the indicated age (n 3). (m), months. In (a), (b) and (c) error bars represent s.e.m.; (*), *p* < 0.05; (**), *p* < 0.01; (***), *p* < 0.001; two tailed Student's t-test. (**d**) Representative picture of SDS-PAGE analysis of MUPs content in urine from mice of each of the indicated genotypes.
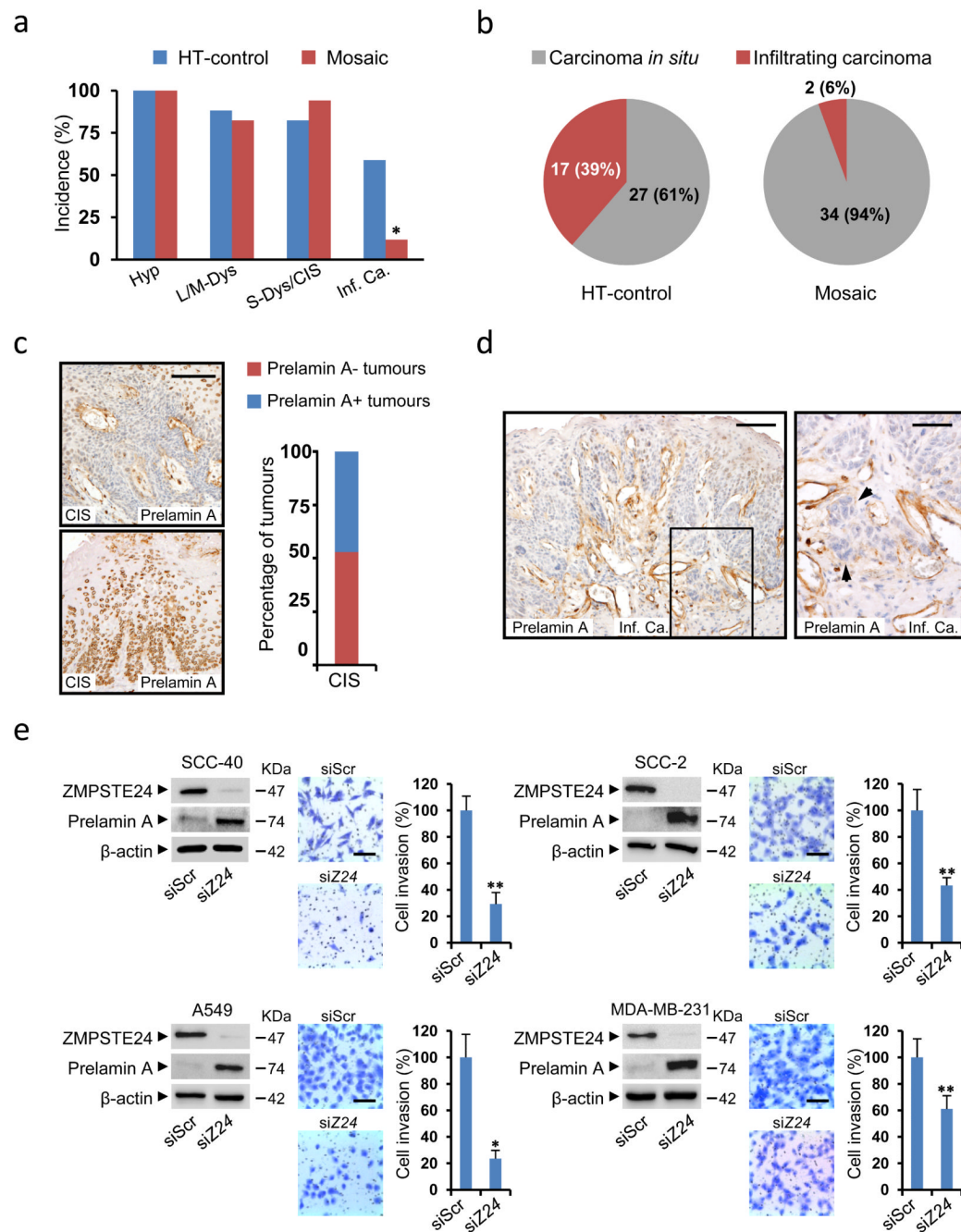
Figure 5. Prelamin A accumulation prevents cancer invasion
(**a**) Percentage of HT-control (n=17) and mosaic (n=17) mice affected by oral lesions with the indicated histology: Hyp, hyperplasia; L/M-Dys, light/moderate dysplasia; S-Dys, severe dysplasia; CIS, carcinoma *in situ*; Inf. Ca., infiltrating carcinoma. (**b**) Number and proportion of *in situ* and infiltrating oral carcinomas in each group. (**c**) Representative photomicrographs of positive (bottom) and negative (top) prelamin A staining in oral CIS from mosaic mice. The percentage of prelamin A positive and negative CIS is plotted. A total of 17 CIS were analyzed by prelamin A immunohistochemistry. Scale bar represents 100 µm. (**d**) Representative photomicrographs of a prelamin A negative infiltrating

carcinoma from a mosaic mouse. Arrowheads point at nests of invasive cancer cells. Scale bars represent 100 μm (left panel) and 50 μm (right panel). (**e**) Effect of *ZMPSTE24* silencing on the invasiveness of SCC-40, SCC-2, A549 and MDA-MB-231 cancer cell lines. Left panels: Western blots showing the accumulation of prelamin A upon *ZMPSTE24* (si*Z24)* vs. scrambled (siScr) silencing. Right panels: Representative pictures and average number of invasive *ZMPSTE24*-interfered and scrambled-treated cells. The assays were carried out at least in triplicate and results are expressed as mean ± s.e.m. (*), $p < 0.05$; (**), $p < 0.01$; Fisher's exact test. Scale bars represent 100 μm.